ELSEVIER

Journal of Nuclear Materials 300 (2002) 255–265

journal of nuclear materials

www.elsevier.com/locate/jnucmat

# The effect of coatings on deuterium retention and permeation in aluminum 6061-T6 APT tritium production tubes

K.L. Hertz *, R.A. Causey, D.F. Cowgill

*Sandia National Laboratories, P.O. Box 969, MS 9402, Livermore, CA 94551-0969, USA*

Received 22 June 2000; accepted 24 September 2001

**Abstract**

The accelerator production of tritium project will utilize spallation neutrons incident on thousands of $^3$He gas filled metal tubes to produce tritium by way of the exothermic $^3$He(n,p)$^3$H reaction. Tritons with energies up to 192 keV and protons with energies up to 576 keV are directly implanted into the tube walls. To minimize tritium retention in the tubes and permeation into the coolant surrounding the tubes, it is desirable to have the implanted tritium migrate back to the inner surface of the tubes and rapidly recombine to be released as $T_2$ and HT. Aluminum alloy (Al 6061-T6) is the primary candidate material for fabrication of the tubes. Aluminum alloy samples implanted with deuterons and protons to fluences as high as $3 \times 10^{22}$ D (and p)/m$^2$ were studied. Deuterium retention was measured by mass spectrometry during thermal desorption. Approximately 10% of the implanted deuterium was retained. Copper, nickel and anodized coatings on aluminum alloy were studied as possible methods of reducing retention and permeation of the tritium. In these experiments, the Cu and Ni coatings reduced the retention significantly, whereas retention increased in the anodized coated sample. © 2002 Published by Elsevier Science B.V.

## 1. Introduction

The concept of the accelerator production of tritium (APT) device is to accelerate protons to very high energies, interact these protons with tungsten to produce spallation neutrons, thermalize the neutrons, and react the thermal neutrons with $^3$He gas to produce tritium. The APT device will contain approximately 8000 thin-walled tubes filled with $^3$He to a pressure of 0.68–0.88 MPa. The exothermic $^3$He(n,p)$^3$H reaction converts the $^3$He gas to tritium with an energy of 192 keV. Depending on the final design for the diameter of the tubes and the $^3$He gas pressure, ≈10–15% of the tritium produced will be injected into the tube walls. Depending on the location of the tubes in the APT blanket, the tritium flux incident on the tube walls will vary between $10^{14}$ and $10^{17}$ T/m$^2$ s with an average of about $5 \times 10^{15}$ T/m$^2$ s. Similarly, the temperature of the tubes will vary between 330 and 370 K. Candidate materials for the fabrication of the APT tubes are Al 6061-T6 and stainless steel (SS 316L). The wall thickness will be between 0.51 and 0.81 mm for the aluminum alloy and between 0.56 and 0.64 mm for stainless steel.

The tritium gas pressure that will exist within the tubes and the continuous tritium injection into the tube walls raise a valid concern about tritium retention in the tube walls and/or permeation through the tubes into the surrounding cooling water. Neither of these conditions is desirable for APT operation. Holdup in the tube walls will make it difficult for APT to meet its production goals and extract the produced tritium from the tube walls. High levels of permeation will necessitate a costly detritiation system for the cooling water.

* Corresponding author. Tel.: +1-925 294 4535; fax: +1-925 294 3231.

*E-mail address:* klhertz@sandia.gov (K.L. Hertz).

0022-3115/02/$ - see front matter © 2002 Published by Elsevier Science B.V.
PII: S0022-3115(01)00707-3

This paper discusses experiments completed at Sandia National Laboratories that utilized a 200 keV accelerator to implant deuterons and a 700 keV accelerator to implant protons into aluminum alloy samples at temperatures and particle fluxes appropriate for APT. Deuterium was used for these experiments, because the migration of deuterium and tritium through materials is very similar [1]. Initial experiments in which only deuterium was implanted demonstrated that the aluminum alloy retains ≈20% of the implanted deuterium [2]. This prompted an investigation into methods to reduce both retention and permeation. One possibility is to coat the inside of the tubes with a material whose characteristics promote the rapid recombination of tritium and protium into the gas at the inner tube surface. Both copper and nickel were examined as possibilities. These materials do not form stable oxides in the APT environment, have high recombination coefficients for tritium and have relatively high tritium diffusivity and solubility. The porous structure of anodized aluminum may aide in the release of tritium, thus this type of coating was tested as well.

The implanted samples were analyzed by several techniques providing significant information on the behavior of the implanted deuterium within the samples. The build-up of deuterium in the near-surface during implantation was measured by D(d,p)T nuclear reaction analysis (NRA). The total deuterium retained within the samples after the implant was measured by a mass spectrometer during thermal desorption. The permeation of deuterium through the sample to the back surface was measured with $D(^3He,p)^4He$ NRA. The formation of blisters and other visual changes in the surface of the samples were identified by SEM. The results of the sample analysis and the potential impact of the results on APT are discussed.

## 2. Motivation

The objective of the implantation experiments was to determine the behavior of tritium in the reference materials for APT tubes under conditions closely resembling those expected for APT operation. The diffusion, solubility, recombination rate, and trapping and bubble formation of tritium with respect to the metal all contribute to the concentration profile of tritium in the sample. The direct implantation of tritium into a metal allows a high concentration of tritium to develop in the implant region dependent on the incident flux and diffusivity of the tritium. The tritium migrates from this area of high concentration toward regions of low concentration at the surface and in the bulk. The concentration of tritium at the surface is dependent on the release rate of tritium from the surface. In most cases, the release rate is limited by the rate at which tritium atoms are able to recombine into molecules and can be defined as the product of the recombination rate coefficient times the square of the tritium concentration immediately below the surface.

Ideally, the tritium injected into the APT tube walls would migrate to the inner surface of the tube and recombine into molecules. Previous accelerator experiments that implanted deuterium into the Al 6061-T6 [2] showed that the aluminum alloy hindered this process. The recombination rate coefficient for hydrogen isotopes in aluminum alloy under the experimental conditions was low, thus the deuterium concentration at the surface and therefore in the bulk was high. Secondly, the low solubility of deuterium in aluminum alloy combined with the deuterium flux used in the experiment promoted the formation of blisters that trapped deuterium within the tube walls. The blisters form when the concentration of deuterium gas exceeds the limit of solubility, and deuterium atoms recombine into molecules at defects in the metal. The concentration of deuterium above the solubility limit will precipitate into bubbles. Significantly larger quantities of hydrogen isotopes can be trapped in bubbles (H/Metal ≈ 0.1) than in solution. Both of these characteristics increase the retention and possibly the permeation of tritium.

This experiment focuses on an attempt to lower tritium retention and permeation in the APT $^3He$ tubes by the application of a thin metal coating to the inside surface of the tubes. There are several effects the coatings may have on the tritium migration. First, if the coating material has a higher recombination rate coefficient for tritium than the bulk material, the tritium release from the surface should be increased, lowering the tritium concentration at the surface and in the bulk. Second, at the interface between the coating and the substrate there is a discontinuity in tritium concentration based on the ratio of the solubility of tritium in the substrate to the solubility of tritium in the coating. A coating with higher tritium solubility than that of the substrate material will help reduce the permeation. The higher solubility also decreases the probability of blister formation. Both copper and nickel have these characteristics.

Recombination rate coefficients are highly affected by surface conditions and impurities, especially oxides. The addition of impurities to the metal surface decreases the recombination rate coefficient by essentially covering sites where the hydrogen can recombine to form $H_2$. Two research groups have measured the recombination rate coefficient for hydrogen in aluminum. Kamada et al. [3] used elastic recoil detection in 1984 to determine the recombination rate coefficient for hydrogen in pure aluminum to be approximately $10^{-36}$ $m^4/s$ at temperatures relevant to APT. In 1992, Hayashi et al. [4] determined the effective recombination rate coefficient for deuterium implanted into pure aluminum to be ap-

proximately $10^{-22}$ $m^4/s$ at 500 K. The high flux implantation, $1 \times 10^{19}$ $D/m^2$ s, used in their experiment is thought to have continuously 'stirred' the oxide layer on the surface creating an environment not relevant to APT. The difference between these two values is 14 orders of magnitude. This stresses the importance of measuring the recombination rate coefficient under APT conditions. Due to the low temperature, low particle flux, and relatively high oxygen potential that will be present in APT, the recombination rate coefficient of tritium in the bare aluminum alloy will most likely be quite low. Both copper and nickel can be used to increase the surface recombination rate of tritium, reducing the concentration at the surface and in the bulk. Wilson et al. [5] measured the recombination rate coefficient for copper to be a constant $6.7 \times 10^{-26}$ $m^4/s$ over the temperature range 575–825 K. Besenbacher et al. [6] determined the recombination rate coefficient for pure nickel to be at least $10^{-27}$ $m^4/s$ at 350 K.

Eichenauer et al. [7–9] calculated the solubility of hydrogen in 99.5% pure aluminum, copper, and nickel from measurements of the diffusivity. The solubility of hydrogen in copper is several orders of magnitude higher than for aluminum at 353 K. Under APT conditions, the formation of bubbles in copper may be possible. As the solubility of hydrogen in nickel is several orders of magnitude higher than copper, blisters are not expected to form under APT conditions.

## 3. Accelerator implants

The $^3He(n,p)^3H$ reaction produces 192 keV tritons and 576 keV protons. These monoenergetic particles are emitted isotropically and at various distances from the tube walls. The particles lose energy in the $^3He$ gas before striking the tube walls resulting in a continuous, linearly decreasing profile of ions injected into the tube walls. The experiments discussed in this paper were designed to simulate these conditions. The 200 keV accelerator was used to implant deuterons with energies of 14, 78, 140, and 200 keV. The 700 keV accelerator was used to implant protons with energies of 150, 225, 300, 375, 450, 525 and 600 keV. The 700 keV accelerator loses stability at energies lower than 150 keV, thus the lowest proton energy implanted was 150 keV. The ions were implanted with an average flux of $1.0 \times 10^{17}$ ions/$m^2$ s to a total fluence of $3 \times 10^{22}$ $D/m^2$ and $3 \times 10^{22}$ p/$m^2$. The low energy ions were implanted to higher fluences and the higher energy ions to lower fluences to simulate the profile expected in APT. Implantation profiles calculated using TRIM [10] are shown in Fig. 1. The implant was initiated with the 14 keV deuterons and progressed through the higher energies, then the protons were implanted beginning with 150 keV. To reach a fluence of $1 \times 10^{22}$ D (and p)/$m^2$ the experiment progressed through three of these cycles, alternating between deuteron and proton implants. The cycles were repeated until the final fluence was reached.

The tritons and protons recoil injected into the APT tube walls will be injected simultaneously. The accelerator implantation of the deuterons and protons alternated, with the protons implanted last. The implantation of the samples took approximately 2 months, therefore the experiments were not repeated implanting protons and then deuterons. The effect of the proton implantation following the deuteron implantation will be discussed in the results section.

The following procedure was used for the daily deuteron and proton implants. A liquid nitrogen cold

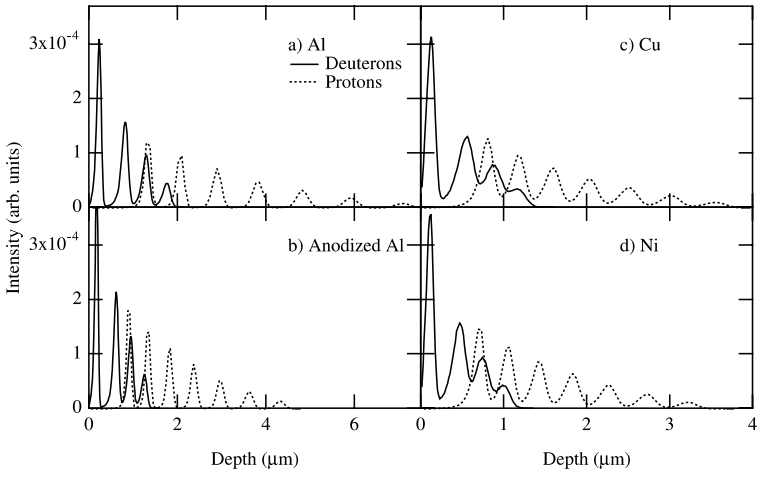


Fig. 1. Deuteron (——) and proton (·····) implant profiles calculated with TRIM [10] in (a) aluminum, (b) anodized aluminum, (c) copper and (d) nickel.

Table 1
The methods used to prepare the implanted samples and the thicknesses of the coatings (the thickness of the Zr getter is given in column 3)

| Sample | Sample preparation/coating thickness | Zr layer |
|---|---|---|
| Bare Al | Al 6061-T6, 0.81 mm thick | 0.63 μm |
| Anodized Al | 17 μm thick anodized coating | |
| Cu coated Al | Electroless electroplating process: 1 min Ni deposition at 372 K 120 min Cu deposition at 316 K 6 μm thick | 0.51 μm |
| Cu coated Al | Electroplated: zincated Cu plating for 7 min at 10 ASF 1 μm thick | |
| Ni coated Al | Electroless electroplating process: zincated 20 min Ni deposition at 361 K 8 μm thick | 0.5 μm |

trap was filled to improve the vacuum and reduce carbon build-up on the samples. Temperature sensors were used to sense the level of liquid nitrogen in and automatically fill the trap throughout the experiment. Then, the samples were heated to 373 K. The ion beam was focused to a quartz viewer for conditioning. A rotating beam profiler aided in the conditioning of a collimated 25 mm diameter beam with <10% deviation in intensity over the entire beam spot and was used to monitor the beam throughout the implants. After the beam was properly conditioned the quartz viewer was removed and a calibrated current integrator measured the beam current incident on the samples located at the bottom of a Faraday cup. The entrance aperature to the Faraday cup was biased to suppress secondary electrons from scattered beam. After the desired fluence was reached, the quartz viewer was inserted into the beam line, the sample heater was turned off, and the liquid nitrogen supply was turned off.

A unique feature of this experiment was a foil ladder used to change the energy of the implanted deuterium without changing the voltage of the accelerator. This allowed energy changes to be easily controlled by a computer and made it possible to run the experiment overnight, decreasing the number of days needed to reach the fluences of interest to APT. The foil ladder was located directly in front of the samples to prevent loss of the beam due to scattering in the foils. The foil ladder consisted of several 99.1% pure aluminum foils of varying thickness including a thick piece of commercial aluminum foil to act as a beam stop. A LabVIEW™ program was designed to monitor the experiment and control the movement of the foil ladder.

The sample holder was designed to allow seven 7.9 mm diameter samples, positioned in a hexagonal array, to be implanted simultaneously. The holder was both electrically and thermally isolated from the beam line. Two calibrated thermocouples were connected to the sample holder to ensure a correct reading of the temperature. One was connected to the temperature controller and was used to regulate the temperature of the sample block. The other thermocouple was touching the backside of one of the samples to give an accurate reading of the sample temperature. The sample temperature was lowered slightly before each increase in proton energy so that the beam heating would not raise the sample temperature above 373 K.

One of the goals of these experiments was to assess the feasibility of applying coatings to the inside of the 3 m long 6.35 mm OD APT tubes. The samples implanted during these experiments are listed in Table 1. The application of nickel coatings was fairly well understood, whereas copper coatings proved much more difficult to apply. The second column describes the method used to apply the coating and the thickness of the coating. These methods of application are thought to be feasible in the 3 m long tubes. The thickness was determined from optical or SEM images of the sample cross-section. The 200 keV deuterons penetrate approximately 1.3 μm and the 600 keV protons penetrate approximately 4 μm into both copper and nickel. Thus, the optimal thickness for the coating was at least 4 μm to ensure that the ions stopped in the coating and did not penetrate into the substrate. The third column lists the thickness of the zirconium getter applied to the back surface of some of the samples. Samples used for thermal desorption analysis did not have a Zr layer applied to the back surface. The zirconium was used to trap deuterium that permeated through the sample. The trapped deuterium was then measured by $D(^3He,p)^4He$ NRA. The zirconium layer must be thinner than the range of 650 keV $^3He$ in zirconium, approximately 1.3 μm, so that the entire thickness of the coating can be profiled. The samples were prepared from the same piece of 0.81 mm thick certified Al 6061-T6. The surfaces were not polished before the implantation in an effort to simulate the as-fabricated surface finish on the inside of the APT tubes as closely as possible.

## 4. Analysis techniques

### 4.1. D(d,p)T nuclear reaction analysis

The deuteron beam is unique in that it can be used to simultaneously implant deuterium and probe the sample

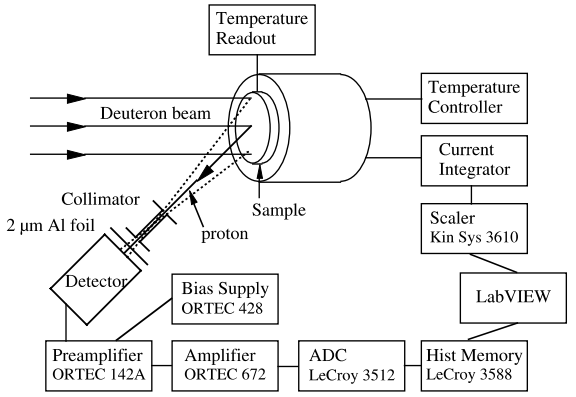


Fig. 2. A diagram of the experimental setup for the D(d,p)T NRA.

to measure the accumulation of deuterium in the implant region. D(d,p)T NRA was used to measure the build-up of implanted deuterium in the near-surface region of the samples during the implant. An array of five silicon detectors measured the protons and tritons emitted from the D(d,p)T reaction during the 200 keV deuteron implants. A schematic diagram of the experimental setup used for the NRA of a single sample is shown in Fig. 2. The deuteron beam was incident normal to the sample and the silicon detector was located at 135° with respect to the beam. A collimator positioned in front of the detector ensured that only particles scattered from a single 49 $mm^2$ sample entered the detector. The dotted lines drawn from the detector to the sample show the boundary of the 33 $mm^2$ area of the sample visible by the detector. The detector subtended a solid angle of 0.018 sr, calculated from the geometry of the experimental setup. The 2 μm thick aluminum foil in front of the detector prevented the low energy backscattered deuterons from entering the detector.

A detailed description of the D(d,p)T analysis technique and the limitations of this method are given in a paper by Cowgill [11]. The analysis converts the measured proton energy spectrum to the deuterium concentration versus depth. The deuteron and proton stopping powers and ranges needed for this conversion were calculated using the computer code TRIM [10]. The depth profiling calculations were calibrated with five preloaded $ErD_2$ samples bombarded by 200 keV deuterons to a fluence of $2 \times 10^{20}$ $D/m^2$. Fig. 3(a) shows the proton spectrum and (b) the resulting deuteron concentration (D atoms/metal atoms) profile for one of the silicon detectors. The channel corresponding to protons emitted from the surface of the sample was chosen by requiring that the calculated concentration be approximately half-maximum at the surface and is indicated by the dotted line through the proton spectrum in Fig. 3(a). Once the surface channel was determined, it remained unchanged for the analysis of the implanted samples. The gradual increase in the deuterium concentration from the surface to about 0.2 μm is due to the depth resolution of these measurements. The depth resolution has several major contributions: the detector resolution, the straggling of the incident deuterons in the sample, the straggling of the outgoing protons in the sample and in the 2 μm aluminum foil in front of the detector,

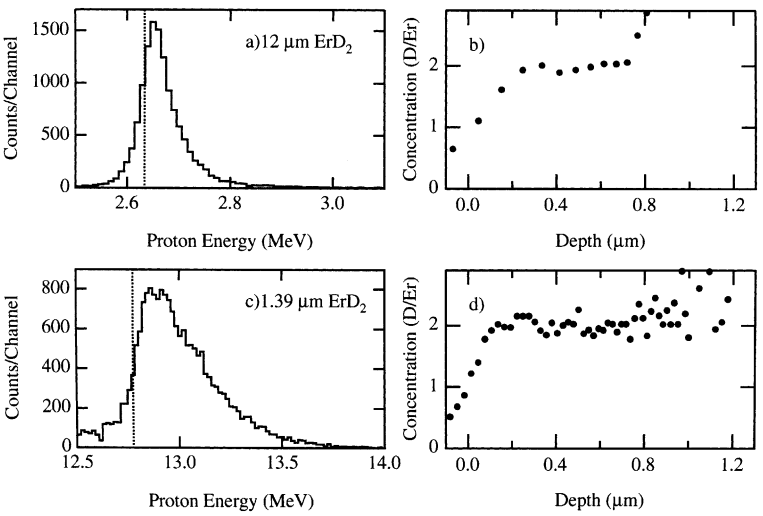


Fig. 3. (a) The proton spectrum resulting from the D(d,p)T nuclear reaction from the bombardment of 200 keV deuterons on a $ErD_2$ sample. The dotted line indicates the surface channel of the profile. (b) The calculated deuteron concentration with respect to sample depth for (a). (c) The proton spectra obtained from the $D(^3He,p)^4He$ nuclear reaction from the bombardment of 650 keV $^3He$ on a $ErD_2$ sample and (d) the calculated deuteron concentration with respect to sample depth for (c).

and the angle of acceptance of the detector. From Fig. 1(a) the range of the 200 keV deuteron is seen to be 1.1 μm. The resolution of the profiling method is only sufficient to depths of ≈0.7 μm, thus calculations beyond that are unreliable.

### 4.2. Thermal desorption spectroscopy

Thermal desorption spectroscopy (TDS) was used to measure the total deuterium retained within the samples after implantation. Only samples without a Zr layer on the back surface were desorbed. A radiant vacuum furnace and mass spectrometer were used to thermally desorb the deuterium from the samples. A sample loader and a moveable sample holder allowed the furnace to remain under vacuum when a new sample was placed in the system; this reduced the amount of background contamination measured by the spectrometer. The mass spectrometer was calibrated preceding each desorption with a $D_2$ standard leak. A programmable temperature controller ramped the temperature of the furnace at a rate of 1 K/s to 903 K, just below the 933 K melting temperature of aluminum. The temperature was maintained at 903 K until desorption of the relevant masses was completed. The desorption rates for $H_2$, HD, $D_2$, and various water and methane molecules (masses 16, 17, 18, 19, and 20) were recorded in a data file for analysis.

### 4.3. $D(^3He,p)^4He$ nuclear reaction analysis

The exothermic $D(^3He,p)^4He$ nuclear reaction was used to measure deuterium permeation through various samples. A 0.5 μm thick zirconium layer applied to the back surface of the samples trapped deuterium that permeated through the sample. The trapped deuterium was measured by $D(^3He,p)^4He$ NRA after each $1 \times 10^{22}$ D (and p)/$m^2$ implant interval. A well-focussed 650 keV $^3He$ beam was incident normal to the sample. An annular silicon detector located at 180° with respect to the beam detected the 12.78–17.11 MeV scattered protons. The area of the detector was 200 $mm^2$ with a 4mm diameter opening through which the $^3He$ beam passed. The detector was shielded on the upstream side by an aluminum aperture held at −200 V to suppress scattered electrons and on the downstream side by a 2 μm thick aluminum foil to prevent low energy back-scattered particles from entering the detector. The detector subtended a solid angle of 0.019 sr. This was calculated from the geometry of the experimental setup and was confirmed using a $^{241}Am$ alpha source. The energy signals from the silicon detector and the integrated current were recorded using LabVIEW™. The proton energy signals were converted to deuteron depth in a manner similar to that used for the D(d,p)T analysis. The cross-section of the $D(^3He,p)^4He$ reaction was taken from measurements by Möller and Besenbacher [12]. The stopping powers and ranges of $^3He$ and protons were calculated using TRIM [10].

The measurement was calibrated with a 1.39 μm thick $ErD_2$ sample. The beam current used for the profiling was $3 \times 10^{16}$ $^3He/m^2$ s (10 nA), therefore beam heating was not a concern. A typical proton spectrum is shown in Fig. 3(c). The channel corresponding to protons scattered from the surface of the sample was chosen by requiring the concentration to be half-maximum at the surface. The surface channel is indicated by the dotted line. The range of 650 keV $^3He$ in the $ErD_2$ is ≈1.5 μm, however the profiling is only accurate to approximately 1.0 μm. This is seen in Fig. 3(d) by the increased scatter in the concentration. The gradual increase in the deuterium concentration from the surface to 0.1 μm is due to the depth resolution of these measurements. A comparison of Fig. 3(b)–(d) shows the increased depth resolution for the $^3He$ profiling compared to the D profiling. The D(d,p)T analysis is restricted by experimental conditions, whereas the $^3He$ profiling is optimized for analysis.

## 5. Results

### 5.1. Near-surface deuterium concentration

The protons emitted from the D(d,p)T nuclear reaction were used to measure the deuterium in the near-surface region of the sample during the implant of the 200 keV deuterons. The spectra were obtained with a collection fluence of $4.76 \times 10^{20}$ D/$m^2$. After converting the proton yield to deuterium concentration, the total deuterium in the near-surface region was calculated by integrating the deuterium concentration over the depth. The integrated totals are plotted versus fluence in Fig. 4. The figure shows a steady increase in deuterium concentration in the near-surface region of all the samples with increasing dose. The anodized coating exhibited an increase in the concentration compared to that for the bare aluminum alloy, whereas both the Cu and Ni coatings showed decreased concentration compared to the aluminum alloy. Due to limitations in the experimental setup, the depth resolution was insufficient to distinguish between deuterium trapped in surface oxides and deuterium trapped in the substrate material.

### 5.2. Deuterium retention

The total deuterium retained within the samples after the implants was measured by TDS. The TDS measurements were completed within a few weeks of the final implants. During the temperature ramp, deuterium was released from the samples in the form of HD, $D_2$, and HDO. The total quantity of deuterium released

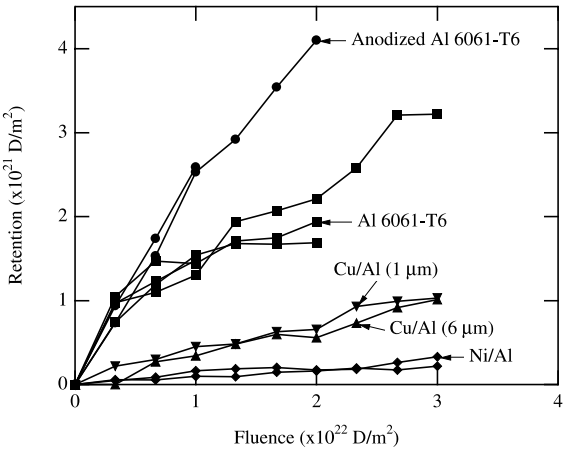


Fig. 4. The total deuterium in the near-surface region of the samples during the implantation of 200 keV deuterons measured by D(d,p)T NRA versus the fluence. The accumulation of deuterium in the copper and nickel coated samples is considerably less than that for the bare and anodized aluminum alloy. Measurements were made for several samples.

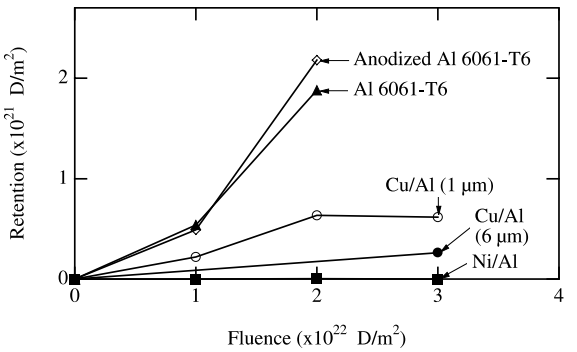


Fig. 5. The total deuterium retention measured by TDS for coated and bare aluminum alloy samples implanted up to fluences of $3 \times 10^{22}$ D (and p)/m$^2$.

from a sample was calculated by integrating the mass spectrometer signals over time and summing the deuterium contributions from the various molecules. The results are listed in Table 2 and the retention versus fluence is plotted in Fig. 5. A few observations can be made from the data. Retention in the bare aluminum alloy and anodized aluminum alloy has not appeared to reach saturation at these fluences. The copper coating successfully decreases the retention and the nickel coating nearly eliminates retention. One should remember that the implant cycles always ended with proton implantations. This may have allowed the diffusing protons to have exchanged with the trapped deuterons allowing deuterium to migrate toward the surface, and thus decreasing the deuterium retention. This exchange and the continued migration of the deuterium to the surface of the samples explains why the deuterium retention throughout the bulk of the sample is less than the deuterium measured in the near-surface region during the implants.

### 5.3. Deuterium permeation

The 0.5 μm zirconium layer on the backside of the samples acted as a trap for permeated deuterium. After each $1 \times 10^{22}$ D (and p)/m$^2$ implant cycle, the zirconium was profiled by the D($^3$He,p)$^4$He nuclear reaction. Spectra with sufficient statistics were obtained with collection fluences of either $5 \times 10^{19}$ or $1 \times 10^{20}$ $^3$He/m$^2$. No deuterium was measured in the zirconium layer on any of the bare and coated aluminum alloy samples, indicating that no deuterium permeated through the samples.

Table 2
The thermal desorption data for the samples (the implant fluence and the total deuterium desorbed as HD, $D_2$, and HDO molecules are listed for each sample)

| Sample | Fluence (D/m$^2$) | $\sum$ HD(D/m$^2$) | $\sum$ $D_2$ (D/m$^2$) | $\sum$ HDO (D/m$^2$) | Total D (D/m$^2$) |
|---|---|---|---|---|---|
| 6061-T6 Al | $1.0 \times 10^{22}$ | $5.40 \times 10^{20}$ | 0 | 0 | $5.40 \times 10^{20}$ |
| | $2.0 \times 10^{22}$ | $1.70 \times 10^{21}$ | $9.08 \times 10^{19}$ | 0 | $1.88 \times 10^{21}$ |
| Electroplated Cu/Al | $1.0 \times 10^{22}$ | $2.21 \times 10^{20}$ | 0 | 0 | $2.21 \times 10^{20}$ |
| | $2.0 \times 10^{22}$ | $6.35 \times 10^{20}$ | 0 | 0 | $6.35 \times 10^{20}$ |
| | $3.0 \times 10^{22}$ | $6.17 \times 10^{20}$ | 0 | 0 | $6.17 \times 10^{20}$ |
| Electroless Cu/Al | $3.0 \times 10^{22}$ | $3.07 \times 10^{20}$ | $8.14 \times 10^{17}$ | 0 | $3.23 \times 10^{20}$ |
| Electroless Ni/Al | $1.0 \times 10^{22}$ | 0 | 0 | 0 | 0 |
| | $2.0 \times 10^{22}$ | $4.86 \times 10^{18}$ | 0 | 0 | $4.86 \times 10^{18}$ |
| | $3.0 \times 10^{22}$ | 0 | 0 | 0 | 0 |
| Anodized Al | $1.0 \times 10^{22}$ | 0 | 0 | $4.92 \times 10^{20}$ | $4.92 \times 10^{20}$ |
| | $2.0 \times 10^{22}$ | 0 | 0 | $2.18 \times 10^{21}$ | $2.18 \times 10^{21}$ |

## 6. Discussion

### 6.1. Bare aluminum

Al 6061-T6 is the base-line material for these experiments. The release of $H_2$, HD, and $D_2$ during thermal desorption of the aluminum alloy samples is shown in Fig. 6. The $H_2$, HD, and $D_2$ spectra all have a narrow peak around 675 K. This peak may be the result of bubbles and blisters forming in the aluminum alloy. The deuteron and proton implantation cycles always ended with protons; therefore the higher $H_2$ peak than $D_2$ peak may be the result of the protons 'washing out' or exchanging with the deuterium trapped in bubbles and blisters. Previous experiments for aluminum alloy using only deuteron beams [2] showed a higher release of $D_2$ and no $H_2$ peak at 675 K. Kamada et al. [13] completed an experiment with successive implants of 25 keV $D_2^+$ and 100 or 140 keV $H_2^+$ into high purity aluminum. They found that the deuterium retained in the sample decreased as the hydrogen fluence increased even though the depth of the implantation of the hydrogen was significantly larger than for the deuterium. Kamada et al. calculated the collisional de-trapping cross-section and found that it was significantly smaller than the measured effects, therefore some other mechanism such as cascade mixing or enhanced diffusion contributed to the reduced deuterium retention [14]. This is consistent with the decrease in deuterium seen here.

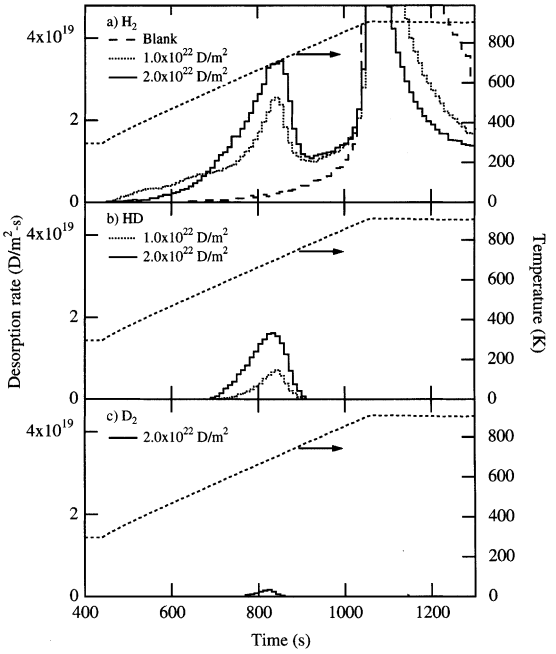


Fig. 6. The thermal desorption spectra for the aluminum alloy samples implanted to $1 \times 10^{22}$ and $2 \times 10^{22}$ D (and p)/m$^2$. The narrow peaks of $H_2$, HD, and $D_2$ at 675 K are due to the release from bubbles.

SEM images taken at 20 000× of the surface of the aluminum alloy sample before implantation (Fig. 7(a)), and after implantation (Fig. 7(b)) show that blisters and cracks were formed during implantation. The NRA (Fig. 4) and TDS (Fig. 5) results also indicate that at a fluence of $3.0 \times 10^{22}$ D/m$^2$ the deuterium retention in the aluminum alloy has not yet reached saturation. Although permeation was not detected up to fluences of $3.0 \times 10^{22}$ D/m$^2$, the 10% deuterium retention is relatively high.

The implantation results obtained from the aluminum alloy samples are supported by other experimental measurements on aluminum alloys. The low surface recombination rate for hydrogen in aluminum results in a high concentration of deuterium in the implantation region even at low fluxes. This high concentration of deuterium combined with the low solubility of deuterium in aluminum would predict the formation of bub-

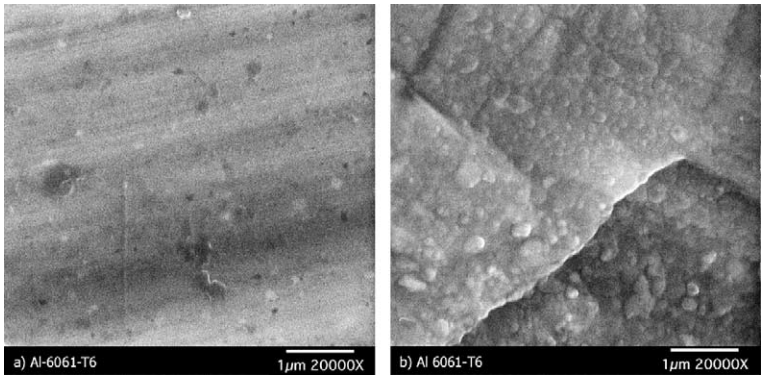


Fig. 7. SEM images at a magnification of 20 000× of aluminum samples (a) before and (b) after the implantation of $2 \times 10^{22}$ D (and p)/m$^2$. Blisters and cracks on the surface due to the implantation are clearly visible.

bles, therefore complicating the modeling of the behavior of hydrogen in aluminum. Extensive research has been completed on hydrogen interactions and bubble formation in aluminum. Myers et al. [15] discuss three hydrogen traps: the surface oxide, vacancy defects caused by irradiation, and $D_2$ bubbles. The irradiation defects have a measured binding enthalpy of 0.52 eV. However, trapping at the surface oxide and in bubbles is significantly stronger than trapping at the irradiation defects. Ades and Companion [16] discuss the formation of blisters as well. Hydrogen is thought to diffuse to voids where it combines to form molecular hydrogen. With increased concentrations the pressure will increase, spreading the void. However, two atoms at interstitial sites adjacent to a vacancy are more stable than a hydrogen molecule. This suggests that hydrogen atoms will collect at sites around the void instead of forming molecules. The stress caused by the slightly negative charge of the atoms around the border of the void may then promote blisters.

### 6.2. Anodized aluminum

The anodized aluminum layer was considered as a possible aide to the release of deuterium due to its porosity. Song et al. [17] studied the permeation of hydrogen through various applied oxide coatings on aluminum. They found that the oxide layers served as permeation barriers rather than release enhancers. However, they concluded that the porosity of anodized aluminum had less of a barrier effect than other applied oxide layers. Song's experiments were performed with a vapor phase permeation technique, not with implanted hydrogen. The implantation of hydrogen directly into the bulk can cause important differences in retention and permeation results.

The thermal desorption spectra for the anodized aluminum samples show that the deuterium was released as HDO, mass 19, shown in Fig. 8. All of the desorption spectra have a peak at about 400 K, including the sample that was not implanted. Since the samples were washed with ethanol before thermal desorption, and the cracking of ethanol produces a TDS peak at mass 19, the low temperature release is attributed to ethanol cracking and the higher temperature release to HDO.

Fig. 5 shows that the deuterium retention in the anodized aluminum is similar to that for the aluminum alloy and has not reached saturation. The deuterium concentration in the near-surface region measured by D(d,p)T analysis during the deuteron implantation is two times greater than that retained after the implants, suggesting that the deuterium is trapped easily in the anodized layer, but that the proton implant promotes the release of the deuterium. Permeation measurements were not made for the anodized aluminum. The anodized layer was not effective in reducing the retention

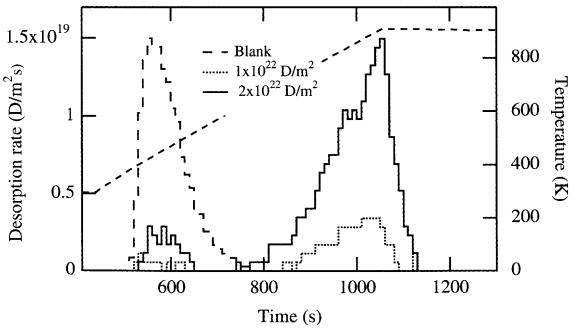


Fig. 8. The thermal desorption spectra of mass 19 for the anodized aluminum samples. The deuterium was desorbed as HDO (mass 19) only, no HD or $D_2$ was measured. The lower peak in the mass 19 spectra is attributed to ethanol used to wash the samples, whereas the higher temperature peak is attributed to HDO.

compared to bare aluminum alloy, therefore it is not suggested for use in APT.

### 6.3. Copper coated aluminum

Two copper coated aluminum alloy samples were studied during these experiments. The electroless electroplated copper sample had a 6 μm thick coating whereas the electroplated copper sample had only a 1 μm thick coating. A comparison of these two samples emphasizes the importance of the thickness of the copper layer. The 6 μm layer ensures that all of the implantation occurs in the copper layer and that the interface between the copper and aluminum alloy may act as a barrier for the permeating deuterium. A thin coating may allow some implantation to occur directly into the aluminum alloy substrate. In this case, the coating provides an oxide free surface to enhance recombination, but does not act as a migration barrier. Inal et al. [18] implanted 3.3, 6.7, and 9.8 μm thick copper coated aluminum samples and found that deuterium retention did decrease with increased coating thickness.

The near-surface deuterium concentration measured by D(d,p)T analysis in both the samples is very similar. However, the total retention measured by TDS in the sample with the 1 μm thick coating is larger than that of the other sample. This suggests that deuterium is being directly implanted into the aluminum alloy through the 1 μm coating and is trapped at the copper–aluminum alloy interface or within the aluminum alloy. The thermal desorption spectra for the release of HD from both of the copper samples implanted to a fluence of $3 \times 10^{22}$ D (and p)/$m^2$ are shown in Fig. 9. No deuterium was released as $D_2$ from the sample with the 1 μm thick copper coating and only a small amount was released

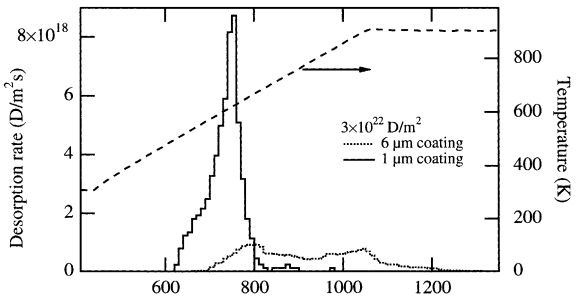


Fig. 9. The thermal desorption spectra of HD for the 1 μm thick and 6 μm thick copper coated aluminum samples.

from the sample with the 6 μm thick copper coating. The broad HD peak (6 μm sample) suggests that deuterium trapped within the sample migrated to the surface where it recombined with a hydrogen atom. The narrow peak (1 μm sample) suggests that the release is from deuterium trapped at the interface or possibly in bubbles formed within the aluminum alloy.

No obvious changes in the surface are seen in SEM images of the two copper coatings, thus the images are not shown. No permeation was detected in the 6 μm coating sample implanted to a fluence of $3 \times 10^{22}$ D (and p)/m$^2$. Permeation was not measured for the other sample. Both coatings were successful in reducing the retention compared to the aluminum alloy sample. However, a coating thicker than the implant range of the deuterons is preferable.

Two research groups experimentally determined trap energies for deuterium in pure copper. Besenbacher et al. [19] investigated the effects of defect trapping on the migration of deuterium in copper. Two traps were found: a 0.22 eV trap associated with self-interstials and a 0.42 eV trap associated with monovacancies and small vacancy clusters. These trap energies result in deuterium release peaks from implanted copper occurring at 250 and 300 K, showing relatively rapid migration at APT temperatures. Wilson et al. [5] implanted 10 keV $D_3^+$ deuterons at a flux of $1 \times 10^{20}$ D/m$^2$ s to a fluence of $1 \times 10^{23}$ D/m$^2$ at room temperature into copper. Two traps were found in the near surface region at 0.6 and 0.9 eV. The 0.9 eV trap may be due to deuterium release from bubbles whereas the 0.6 eV trap may be due to deuterium-vacancy traps. The traps were measured using TDS.

Johnson and Armstrong [20,21] found that blisters form rapidly in copper at a fluence of $7 \times 10^{22}$ D/m$^2$. Their experiment was performed with polycrystalline copper samples heated to 350 K and bombarded with a 200 keV deuteron beam at a flux of $\approx 9 \times 10^{18}$ D/m$^2$ s. After blisters formed, the deuterium concentration in the blistered area stayed constant. This was measured by D(d,p)T NRA during implantation. They found that the critical dose for blistering in Cu is about 1 at.% deuterium. Blisters were not formed during this experiment, but they may form at the fluences reached by APT.

### 6.4. Nickel coated aluminum

The experimental results for the nickel coated aluminum alloy samples appear very promising. The application of an electroless nickel coating is a well understood process and is easier to control than the electroless electroplating copper deposition process. No deuterium was released during the thermal desorption as either HD or $D_2$, thus the spectra are not shown. Similar experiments were completed that implanted nickel coated stainless steel samples. These samples were heated to 1273 K during TDS and again no deuterium was measured. SEM images of the nickel surface up to 20 000× resolution show no visible change in the metal due to the proton and deuteron implants. The D(d,p)T NRA of the near-surface reveals small amounts of deuterium building up in the near-surface region during the deuterium implantation. The absence of deuterium in the TDS spectra indicates that the deuterium is released, possibly by the implantation of the protons after the deuterons. No permeation was measured in the sample implanted to $3 \times 10^{22}$ D (and p)/m$^2$. The nickel coating is successful at reducing the amount of retained deuterium to negligible amounts. Nickel coated aluminum alloy appears to be a strong candidate for minimizing tritium retention in the APT tubes, although testing under actual irradiation conditions is needed for confirmation.

Besenbacher et al. [6] investigated the effects of defect trapping on the migration of deuterium in nickel. They reported two trap energies for deuterium attachment to defects produced by implantation. The first trap, with an energy of 0.24 eV, is associated with the attachment of deuterium to a single vacancy. The other trap was reported at 0.43 eV, associated with deuterium attachment to multiple-vacancy defects. Relatively rapid migration of the trapped deuterium was seen for temperatures between 250 and 350 K. For both trap energies, the deuterium would be expected to remain mobile at the temperatures relevant to APT.

## 7. Implications to APT

The implantation of deuterons and protons into various aluminum alloy samples was performed to test possible candidate materials for APT $^3$He tubes. Bare aluminum alloy retained approximately 10% of the implanted deuterium prompting the investigation of copper, nickel, and anodized coatings for minimizing

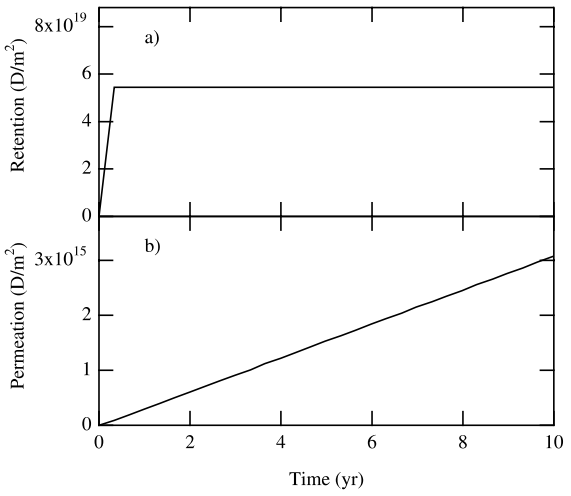


Fig. 10. Calculations using the computer code DIFFUSE to predict (a) the retention and (b) the permeation of nickel coated aluminum tubes over 10 years of APT operation.

retention. A nickel coating approximately 6 μm thick on an aluminum alloy substrate proved successful in substantially reducing the retention.

DIFFUSE code [22] calculations for the nickel coated sample were completed to determine the implications of the experimental data to APT. The calculations were performed assuming that the average tritium flux for APT is $5 \times 10^{15}$ T/m$^2$ s and the total wall area of the $^3$He tubes is 1200 m$^2$. These values allow for 950 g T/year to be incident on the tube walls. Fig. 10 shows the results of retention and permeation calculations for nickel coated aluminum over 10 years of continual APT operation. The calculations predict that within a few months the tritium retention reaches saturation. The calculations also predict that after 10 years of operation, only 1 g of tritium is predicted to be retained in the APT tube walls. The amount of tritium predicted to permeate through the APT tube walls is only $2 \times 10^{-5}$ g for the nickel coated aluminum. These results indicate that nickel coated aluminum tubes should be effective for use in APT, although actual testing in a prototypic proton and neutron flux is needed to support these results.

## Acknowledgements

This work was funded by the Accelerator Production of Tritium Project under USDOE contract W-7405-ENG-36.

## References

[1] J. Völkl, G. Alefeld, in: G. Alefeld, J. Völkl (Eds.), Hydrogen in Metals I, Topics in Applied Physics, vol. 28, Springer, Berlin, 1978.
[2] D.F. Cowgill, R.A. Causey, Mater. Charact. 43 (1999) 169.
[3] K. Kamada, A. Sagara, N. Sugiyama, S. Yamaguchi, J. Nucl. Mater. 128&129 (1984) 664.
[4] T. Hayashi, K. Okuno, K. Yamanaka, Y. Naruse, J. Alloys Compounds 189 (1992) 195.
[5] K.L. Wilson, R.A. Causey, M.I. Baskes, J. Kamperschroer, J. Vac. Sci. Technol. A 5 (1987) 2319.
[6] F. Besenbacher, J. Bottiger, S.M. Myers, J. Appl. Phys. 53 (1982) 3536.
[7] W. Eichenauer, A. Pebler, Z. Mettallkd. 48 (1957) 373.
[8] W. Eichenauer, K. Hattenbach, A. Pebler, Z. Metallkd. 52 (1961) 682.
[9] W. Eichenauer, W. Loser, H. Witte, Z. Mettallkd. 56 (1965) 287.
[10] J.F. Ziegler, J.P. Biersack, U. Littmark, in: The Stopping and Range of Ions in Solids, vol. 1, Pergamon, New York, 1985.
[11] D.F. Cowgill, Nucl. Instrum. and Meth. 145 (1977) 507.
[12] W. Möller, F. Besenbacher, Nucl. Instrum. and Meth. 168 (1980) 111.
[13] K. Kamada, A. Sagara, S. Yamaguchi, Radiat. Eff. Lett. 85 (1985) 255.
[14] S.M. Myers, Nucl. Instrum. and Meth. 168 (1980) 265.
[15] S.M. Myers, F. Besenbacher, J.K. Norskov, J. Appl. Phys. 58 (1985) 1841.
[16] H.F. Ades, A.L. Companion, Surf. Sci. 177 (1986) 553.
[17] W. Song, J. Du, Y. Xu, B. Long, J. Nucl. Mater. 246 (1997) 139.
[18] M.Y. Inal, M. Alam, K. Kurz, D.F. Cowgill, R.A. Causey, J. Nucl. Mater. 278 (2000) 164.
[19] F. Besenbacher, B. Bech Nielsen, S.M. Myers, J. Appl. Phys. 56 (1984) 3384.
[20] P.B. Johnson, T.R. Armstrong, Nucl. Instrum. and Meth. 148 (1978) 85.
[21] P.B. Johnson, T.R. Armstrong, Appl. Phys. Lett. 31 (1977) 325.
[22] M.I. Baskes, J. Nucl. Mater. 92 (1980) 318.